

Raman spectroscopy-enhanced IIT: *In situ* analysis of mechanically stressed polycrystalline Si thin films

Yvonne B. Gerbig, Research Associate^{a,b}

Chris A. Michaels, Research Chemist^a

Robert F. Cook, NIST Fellow^a

^aNational Institute of Standards and Technology (NIST), Material Measurements Laboratory, 100 Bureau Drive, Gaithersburg, MD 20899, USA

^bUniversity of Maryland, Department of Mechanical Engineering, College Park, MD 20472, USA

ABSTRACT

Exposed to mechanical stress, semiconductor materials may phase transform, resulting in changes of crystallographic structure and material properties, rather than deform by plastic flow. As a consequence, prediction of the state and distribution of strain in semiconductors has become crucial for the evaluation of performance and reliability of structures made of these materials. Indentation-induced phase transformation processes were studied by *in situ* Raman imaging of the deformed contact region of silicon, employing a Raman spectroscopy-enhanced instrumented indentation technique (IIT). This is, to our knowledge, the first sequence of Raman images documenting the evolution of the strain fields and combined changes in the phase distributions of a material under contact load.

KEYWORDS: Indentation, *in situ*, Raman imaging, phase transformation, silicon

INTRODUCTION

Silicon (Si) in its pristine diamond cubic (dc) phase can be transformed to different crystallographic structures through the application of mechanical stress.[1] Given its importance to electronic devices and microelectromechanical systems and given that modifications of the Si crystallographic structure are connected to its performance related properties, phase transformations have been intensively studied. At hydrostatic pressures of 10 GPa to 16 GPa, Si undergoes a nonmetallic-metallic transition, as the dc structure of Si-I transforms to the denser body centered tetragonal (bct) β -tin structure of the Si-II phase.[2-4] Further compression leads to a sequence of transitions to other crystallographic phases according to several theoretical studies and quasi-hydrostatic diamond anvil cell (DAC) experiments.[1] Shear stress is critical in the initiation of phase transitions [5,6] and has been reported to lower the threshold pressure for the phase transformation in monocrystalline Si [7]. Furthermore, it has been speculated that shear stress may promote the formation of phases not observable under hydrostatic conditions.[8,9] Simulation studies suggest the crystal lattice of dc Si transforms into various bct structures with sixfold (β -tin) and fivefold coordination (bct5) under the presence of shear stress during loading.[10-14]

Instrumented indentation technique (IIT) has been widely used to investigate the phase transformation of Si under the presence of shear stress. However, in conventional indentation experiments on Si, the structure and phase of the material is probed only after the completion of the indentation test (*ex situ*), which leaves the exact path of transformation to conjecture, as the presence of intermediate phases cannot be directly observed. In order to analyze the indentation-induced phase transformation *in situ*, auxiliary characterization techniques must be employed in indentation studies. Raman spectroscopy has become a versatile tool, enabling determination of the kinetics and physics involved in the mechanical deformation of materials at the crystallographic and molecular level (*e.g.*, strain build-up in crystal lattices, phase transformations, and changes in crystallinity). The utility of IIT and Raman spectroscopy has led researchers at NIST to explore the combination of these methods for *in situ* measurements, Raman spectroscopy-enhanced IIT, and to develop an indentation device that is coupled with a Raman microscope to conduct spectroscopic and optical analysis (probing and mapping) of mechanically strained regions of transparent samples under contact loading.[15]

In this study, Raman spectroscopy-enhanced IIT in a laser scanning Raman imaging configuration is employed to study *in situ* the generation and evolution of the phase transformation of Si under contact load. The experimental findings are compared to relevant simulations and contact models. This is, to our knowledge, the first sequence of Raman images of a material held under contact load and undergoing phase transformation induced by mechanical deformation.

EXPERIMENTAL DETAILS

Experimental setup

The *in situ* Raman mapping experiments were performed using an instrumented indentation device developed at NIST [15] that is coupled with a laser scanning Raman microscope to conduct *in situ* spectroscopic analyses of mechanically deformed regions of optically transparent materials under contact loading.

The force transducer of the indentation device allows adjustment of experimental parameters, such as indentation loads and (un)loading rates. An incorporated displacement sensor allows for collection of force-displacement data comparable to conventional IIT devices. The indentation device, along with a specimen holder featuring an aperture in the center, are mounted on the X-Y translation stage of an inverted optical microscope that is configured for Raman microscopy, allowing optical access to the mechanically deformed regions of transparent samples.

The Raman microscope has been described in considerable detail elsewhere [15], only a brief discussion of the general set up of recent modifications will follow. Laser scanning capability has been added that enables the acquisition of Raman images of the specimen while held under constant load. These images are generated by raster scanning the beam across the sample region of interest while acquiring Raman spectra at each pixel. Image maps can then be constructed on the basis of parameters of particular spectral features (*e.g.*, peak width or amplitude). The optical arrangement used is conventional for laser scanning microscopes in which two galvanometer scan mirrors (X,Y) are co-located at a plane conjugate to the microscope objective pupil in a conventional 4f imaging system. It is worth noting that this approach, the principal advantage of which is the rapid scan speed, is unusual in Raman microscopy where slow spectral acquisition times are the typical bottleneck. In this case however, the advantage of scanning the laser beam lies in the avoidance of moving the sample and indenter as would be required in a sample scanning configuration. Such movement would undoubtedly compromise the measurement stability and the quality of the force and displacement measurements. The conversion between the angular motion of the galvanometer and the beam displacement in the focal plane is calibrated using a Ronchi grating. A Labview [16] program is used to coordinate the motion and hold periods for the galvanometers and the spectral acquisition by the CCD (charge-coupled device) camera.

Test specimen

The *in situ* mapping experiments were performed on a Si on sapphire (SoS) specimen (manufacturer: Valley Design Corp., Vera Cruz, CA) [16], which is comprised of a Si(100) film epitaxially grown on a sapphire (r-plane) substrate with both sides polished. The thicknesses of film and substrate were $600 \text{ nm} \pm 60 \text{ nm}^1$ and $530 \text{ } \mu\text{m} \pm 50 \text{ } \mu\text{m}^1$, respectively. The $\langle 001 \rangle$ direction of the Si film was rotated away from the substrate normal by $5^\circ \pm 1^\circ$. The sample (20 mm x 20 mm) was cut from a SOS wafer along with a slight misalignment of $3.5^\circ \pm 1^\circ$ with respect to the directions $\langle 110 \rangle$ and $\langle 1\bar{1}0 \rangle$ of the film, as shown by electron backscattering diffraction measurements.

Mapping experiment

A series of Raman images from the contact region between indenter tip and SoS sample were collected for increasing contact loads in stepped indentation experiments. In these tests, the indenter probe was brought into contact with the sample and a load of 40 mN applied and held constant for the time required to collect the Raman image of the region of interest (ROI). The applied indentation force was then increased (loading rate 6 mN/s) to 80 mN and a second Raman image of the same ROI was acquired. The indentation loads were further increased twice more (to 120 mN and 200 mN, loading rate 6 mN/s) and another Raman image was recorded each time. The indenter probe used in the experiments was a conospherical tip made of diamond. The effective radius of tip curvature as a function of indentation depth was determined prior to the mapping experiments based on to the procedure described in ref.[17]

To collect a Raman image, an ROI of $10 \text{ } \mu\text{m} \times 10 \text{ } \mu\text{m}$ was scanned. Twenty individual spectra were collected at evenly spaced locations along the $10 \text{ } \mu\text{m}$ scan range in each direction, generating a 20 pixels x 20 pixels Raman image. The collection time for an individual Raman spectrum was set to 15 s. Although these images may take several hours to acquire, tests of displacement and force stability have been performed that indicate that the system is sufficiently robust to perform such measurements. The estimated depth of field for the collection of Raman photons was about $10 \text{ } \mu\text{m}$. The illumination power of the 785-nm light source was set to 5 mW at the sample surface.

¹ Uncertainties represent manufacturer specifications.

² Uncertainties represent intrinsic measurement errors and mounting errors.

Analysis of Raman spectra

The individual Raman spectra (examples are shown in Fig. 1) were fitted employing a multiple-peak model with Pearson VII functional form for the observed peaks and an iterative optimization routine available in the Peak Analyzer function of the commercial software OriginPro 9 [16] to determine position of the center frequency, height and FWHM (full width at half maximum) of the various peaks. To facilitate the fitting procedure, the bounding conditions summarized in Table 1 were applied to the multiple-peak model.

Determination of the contact pressure and indentation strain

To facilitate the analysis of the experimental data, it is necessary to convert the indentation force (specific to the experimental set-up) to the more “generalized” parameter of average contact pressure. The mean contact pressure p_i at the indentation force F_i (at which a Raman image was recorded) was calculated using the following equation:

$$p_i = F_i / (\pi \cdot a_{c,i}^2) \quad (1)$$

where $a_{c,i}$ is the radius of the circle of contact at the force F_i . The contact radius $a_{c,i}$ was determined at a specific indentation force according to the approach employed by Weppelmann *et al.*[18]

$$a_{c,i} = \sqrt{R_i^2 - (R_i - h_{p,i})^2} \quad (2)$$

where R_i is the effective radius of indenter tip curvature and $h_{p,i}$ is the plastic deformation at the indentation force F_i . The plastic deformation $h_{p,i}$ at the indentation force F_i was calculated with the following equation:

$$h_{p,i} = h_i - \frac{\delta_i}{2} \quad (3)$$

where h_i is the total displacement and δ_i is the elastic deformation at the indentation force F_i . The elastic deformation δ_i at the indentation force F_i was calculated with the following equation:

$$\delta_i = h_i - h_{r,i} \quad (4)$$

where h_i is the total displacement and $h_{r,i}$ is the residual displacement at the indentation force F_i . The values for F_i , h_i and $h_{r,i}$ were determined from the force displacement data recorded during the indentation test.

The indentation strain ε_i was estimated using the following equation:

$$\varepsilon_i = h_i / t \quad (5)$$

where h_i is the indentation depth at the indentation force F_i and t is the film thickness.

As can be seen from the calculated values for p_i and ε_i given in Table 2, the strain increases significantly with greater indentation forces, whereas the average contact pressure changes only slightly.

RESULTS AND DISCUSSION

Figure 1 shows two Raman spectra, one of which is taken outside the contact zone between indenter probe and sample and the other inside the contact zone under the first contact load. The spectrum taken outside the contact zone is representative of the pristine SoS featuring three peaks. Peak 1 observed at 522 cm^{-1} is associated with first-order phonon of the dc phase of Si.[19,20] The peaks located at 378 cm^{-1} and 418 cm^{-1} (peaks 2 and 3) can be assigned to the E_g and A_{1g} modes of the sapphire substrate, respectively.[21] In the center of the contact region, significant changes in the Raman spectrum of the SoS sample were observed: Peak 4 appeared in the spectrum at 535 cm^{-1} and formed a shoulder on the right-hand side of the dc peak. Peak 5 emerged at around 370 cm^{-1} forming a shoulder on the left-hand side of the sapphire E_g mode. As neither of those peaks seems to be associated with the dc Si structure or sapphire, their presence is a manifestation of phase transformation processes in the contact zone at the first contact load (p_i : 5.8 GPa, ε_i : 0.25). The contact pressure of 5.8 GPa is much less than the values (10 GPa to 16 GPa) for the primary phase transformation of single crystal Si reported in quasi-hydrostatic DAC tests.[2-4] However, it confirms previous suggestions that a combination of isotropic compressive and shear strains (as in case of indentation) induces phase transformation at much smaller stresses than those required for compression alone (as in DAC test) in semiconductors.[2,7] Also, our observation is in good agreement with a recently published model for the stress-induced phase transformation of micro-crystalline Si films, which predicts a primary phase transformation event at a contact stress of 6.4 GPa and contact strain of about 0.2.[22]

In a previous study [23], the shift of the Raman peaks 4 and 5 as a function of contact pressure were investigated and compared to data available in the literature. In this comparison, the wavenumber shift for peak 5 aligned reasonably well with data for the transverse optical (TO) mode of β -tin reported for quasi-hydrostatic compression.[24-27] However, in indentation simulations (compressive stress + shear strain), the formation of another phase, bct5 was observed. [11-14] Two Raman-active modes with E_g and A_{1g} symmetries were predicted for the bct5 phase with wavenumbers of 520 cm^{-1} and 340 cm^{-1} . [8,28] The calculated E_g frequency for the bct5 phase is in the wavenumber range of peak 5, suggesting the formation of this phase in the contact zone. The wavenumbers for the A_{1g} mode of bct5 and the TO mode of β -tin are similar, which makes an unambiguous assignment of peak 5 to either of these phases extremely difficult. It was assumed that both phases were present in the contact zone, as recent simulations predict the concurrent transformation of the dc phase to β -tin and bct5 structures during indentation loading.[10-14] To determine unequivocally the formation of β -tin in the contact region, the

occurrence of the longitudinal optical mode for β -tin has to be verified, which is located at around 120 cm^{-1} [24,27] and currently outside the detection range of the experimental set up.

Images assembled from the hyperspectral Raman data cube are summarized in Figure 2 for peak 1 (amplitude and wavenumber) and peaks 4 and 5 assigned to the newly formed, high-pressure phases (wavenumber only) for the different contact loads. Peak 2 and 3 originating from the substrate were considered as not being relevant for this study. As can be seen in Figure 2, the center of the contact region was not exactly aligned with the center of the scan area, so that, unfortunately, the affected region was not entirely mapped, especially at greater indentations forces (strains). However, important conclusions and insights can be drawn from these partial maps.

The low intensity of peak 1 indicates where the phase transformation from the dc phase to high-pressure phases has taken place, as it correlates with the occurrence of peaks 4 and 5 in the wavenumber maps.³ The wavenumber maps also show a circular, isotropic distribution of the high-pressure phases (at least in lateral direction) for the indented polycrystalline Si, which is different from the pronounced anisotropic phase distribution found in residual indentations on monocrystalline Si. [6] The phase (bct5) associated with peak 4 covers a larger portion of the contact area than the phases associated with peak 5 at the first contact load, which is presumably due to the fact that the bct5 phase is formed earlier than the β -tin phase [23,29]. The structure associated with peak 4 continues to occupy a larger portion of the deformed area than the Si phases associated with peak 5 even as the indentation experiment progresses, making it the predominant of the high pressure phases.

With increasing indentation strain (the average contact pressure changes only marginally), the region of reduced peak-1 intensity and the areas where peaks 4 and 5 were detected, grow larger, indicating that an increasing portion of the dc structure in the contact area was transformed to high pressure phases. This seems to give experimental evidence for previous predictions regarding the shear strain being the critical factor in initiating phase transformation rather than the compressive stress.[5,7]

As shown in Figure 2, the wavenumbers of the analyzed Raman modes shifted (significantly) within the deformed area. The wavenumber of the dc Raman peak is shifted to larger wavenumber within the center of the contact zone, indicating the exposure of this phase to compressive stress.[30] However, with greater contact loads, the dc phase seems to relax (less compressively stressed) as the relative Raman shift of this phase decreases in the contact zone. At the same time, the relative Raman shifts for peaks 4 and 5 increases, as the further indentation-induced stresses and strains are compensated by the deformation of the expanding, newly formed phases rather than the diminishing dc structure in the contact zone. As result, the region of the highest Raman shifts of the high-pressure phases enlarges in the center of the contact zone. For peaks 4 and 5, the Raman modes harden from the edge towards the center of the contact area.

CONCLUSION

Indentation-induced phase transformation processes were studied by *in situ* Raman imaging of the deformed contact region of Si, employing a Raman spectroscopy-enhanced instrumented indentation technique (IIT). The evolution of the stress field and the distribution of the high-pressure phases generated in the transformation processes were qualitatively analyzed as a function of the contact conditions. The reported *in situ* experiments provide insights to the transformation processes in Si during loading, confirming and providing the experimental evidence of some of the previous assumptions made on this subject. In this context, the developed experimental setup coupling indentation with *in situ* Raman microscopy has shown its potential in advancing the understanding of the deformation mechanisms.

REFERENCES

- [1] Mujica, A., Rubio, A., Munoz, A., Needs, R.J., High-pressure phases of group-IV, III-V, and II-VI compounds, *Rev. Modern Phys.* 75, 863-913, 2003.
- [2] Gupta, M.C., Ruoff, A.L., Static compression of silicon in the [100] and in the [111] directions, *J. Appl. Phys.* 51(2) 1072-1075, 1980.
- [3] Jamieson, J.C., Crystal structures at high pressures of metallic modifications of silicon and germanium, *Science* 139(3556), 762-764, 1963.
- [4] Hu, J.Z., Merkle, L.D., Menoni, C.S., Spain, I.L., Crystal data for high-pressure phases of silicon, *Phys. Rev. B* 34(7), 4679-4684, 1986.
- [5] Cheong, W.C.D., Zhang, L.C., Stress criterion for the β -tin transformation in silicon under indentation and uniaxial compression, *Key Eng. Mater.* 233-236 603-608, 2003.
- [6] Gerbig, Y.B., Stranick, S.J., Cook, R.F., Direct observation of phase transformation anisotropy in indented silicon studied by confocal Raman spectroscopy, *Phys. Rev. B* 83(20), 205209, 2011.
- [7] Gilman, J., Shear-induced metallization, *Philos. Mag.* B 67(2), 207-214, 1993.

³ The areas colored in black in the frequency plots for peaks 4 and 5 indicate that no signal for the particular peak was collected at these locations.

- [8] Boyer, L.L., Kaxiras, E., Feldman, J.L., Broughton, J.Q., Mehl, M.J., New low-energy crystal structure for silicon, *Phys. Rev. Lett.* 67(6), 715-718, 1991.
- [9] Mylvaganam, K., Zhang, L.C., Eyben, P., Mody, J., Vandervorst, W., Evolution of metastable phases in silicon during nanoindentation: mechanism analysis and experimental verification, *Nanotechnology* 20, 305705, 2009.
- [10] Eyben, P., Clemente, F., Vanstreels, K., Purtois, G., Clarysse, T., Duriau, E., Hantschel, T., Sankaran, K., Mody, J., Vandervorst, W., Mylvaganam, K., Zhang, L., Analysis and modeling of the high vacuum scanning spreading resistance microscopy contact on silicon, *J. Vac. Sci. Technol. B* 28(2), 401-406, 2010.
- [11] Kim D.E., Oh, S.I., Deformation pathway to high-pressure phases of silicon during nanoindentation, *J. Appl. Phys.* 104, 013502 (2008).
- [12] Lin, Y.-H., Jian, S.-R., Lai, Y.-S., Yang, P.-F., Molecular dynamics simulations of nanoindentation-induced mechanical deformation and phase transformation in monocrystalline silicon, *Nanoscale Res. Lett.* 3, 71-75, 2008.
- [13] Sanz-Navarro, C.F., Kenny, S.D., Smith, R., Atomistic simulations of structural transformations of silicon surfaces under nanoindentation, *Nanotechnology* 15, 692-697, 2004.
- [14] Smith, G.S., Tadmor, E.B., Bernstein, N., Kaxiras, E., Multiscale simulations of silicon nanoindentation, *Acta mater.* 49, 4089-4101, 2001.
- [15] Gerbig, Y.B., Michaels, C.A., Forster, A.M., Hettenhouser, J.W., Byrd, W.E., Morris, D.J., Cook, R.F., Indentation device for in situ Raman spectroscopic and optical studies, *Rev. Sci. Instrum.* 83, 125106, 2012.
- [16] Any mention of commercial products within this paper is for information only; it does not imply recommendation or endorsement by NIST.
- [17] Bushby, A.J., Jennet, N.M., Determining the area function of spherical indenters for nanoindentation, *Mat. Res. Soc. Symp.* 649, Q7.17.1-Q7.17.6, 2001.
- [18] Weppelmann, E.R., Field, J.S., Swain, M.V., Observation, analysis, and simulation of the hysteresis of silicon using ultra-micro-indentation with spherical indenters, *J. Mater. Res.* 8(4), 830-840, 1993.
- [19] Aggarwal, R.L., Farrar, L.W., Saikin, S.K., Aspuru-Guzik, A., Stopa, M., Polla, D.L., Measurement of the absolute Raman cross section of the optical phonon in silicon, *Solid State Communications* 151, 553-556, 2011.
- [20] Windl, W., Pavone, P., Karch, K., Schütt, O., Strauch, D., Giannozzi, P., Baroni, S., Second-order Raman spectra of diamond from ab initio phonon calculations, *Phys. Rev. B* 48 (5), 3164-3170, 1993.
- [21] Watson Jr, G.H., Daniels, W.B., Wang, C.S., Measurement of Raman intensities and pressure dependence of phonon frequencies in sapphire, *J. Appl. Phys.* 52, 956-958, 1981.
- [22] Han, C.-F., Lin, J.-F., The model developed for stress-induced structural phase transformations in micro-crystalline silicon films, *Nano-Micro Letters* 2(2) 68-73, 2010.
- [23] Gerbig, Y.B., Michaels, C.A., Forster, A.M., Cook, R.F., In situ observation of the indentation-induced phase transformation of silicon thin films, *Phys. Rev. B* 85(10), 104102, 2012.
- [24] Olijnyk, H., Raman scattering in metallic Si and Ge up to 50 GPa, *Phys. Rev. Lett.* 68(14), 2232-2234, 1992.
- [25] Chang, K.J., Cohen, M.L., Solid-solid phase transitions and soft phonon models in highly condensed Si, *Phys. Rev. B* 31(12), 7819-7826, 1985.
- [26] Lewis S.P., Cohen, M.L., Theoretical study of Raman modes in high-pressure phases of Si, Ge, and Sn, *Phys. Rev. B* 48(6), 3646-3653, 1993.
- [27] Gaál-Nagy, K., Schmitt, M., Pavone, P., Strauch, D., Ab initio study of the high-pressure phase transition from the cubic-diamond to the β -tin structure of Si, *Comput. Mater. Sci.* 22, 49-51, 2001.
- [28] Kaxiras, E., Boyer, L.L., Energetics of large lattice strains: application to silicon, *Phys. Rev. B* 50(3), 1535-1540, 1994.
- [29] Hale, L.M., Zhou, X., Zimmerman, J.A., Moody, N.R., Ballarini, R., Gerberich, W.W., Phase transformations, dislocations and hardening behavior in uniaxially compressed silicon nanospheres, *Comp. Mater. Sci.* 50, 1651-1660, (2011).
- [30] De Wolf, I., Micro-Raman spectroscopy to study local mechanical stress in silicon integrated circuits, *Semicond. Sci. Technol.* 11(2), 139-154, 1993.

TABLES

Table 1: Bounding conditions applied in fitting model of the Raman spectra.

Fitting parameter	Peak 1	Peak 2	Peak 3	Peak 4	Peak 5	Peak 6	Peak 7
Frequency (cm^{-1})	510 to 530	290 to 310	415 to 420	375 to 380	525 to 550	340 to 380	250 to 300
FWHM	1 to 50	1 to 50	1 to 20	1 to 20	1 to 50	1 to 50	1 to 300

Table 2: Values for average contact pressure p_i and indentation strain ε_i calculated from the indentation data at indentation forces F_i , at which Raman images were collected.

	Image 1	Image 2	Image 3	Image 4
F_i (mN)	44	83	122	201
p_i (GPa)	5.8	6.3	6.4	6.4
ε_i	0.25	0.38	0.51	0.72

FIGURE CAPTIONS

FIG 1: Grey scale image showing the distribution of the intensity of peak 1. The dark colored circular area marks the contact region between indenter tip and SoS sample. Raman spectra taken at the indicated spots show the difference in the Raman modes observed outside the contact region and inside the contact region. The spectra are offset along the intensity axis for better illustration.

FIG 2: Raman maps imaging the distribution of intensity (peak 1 only) and wavenumber of particular Raman bands as a function of contact load (expressed in indentation force F_i , contact pressure p_i and indentation strain ε_i) (a) F_i : 44 mN, p_i : 5.8 GPa, ε_i : 0.25, (b) F_i : 83mN, p_i : 6.3 GPa, ε_i : 0.38, (c) F_i : 122 mN, p_i : 6.4 GPa, ε_i : 0.51 , (d) F_i : 180 mN, p_i : 6.4 GPa, ε_i : 0.72. The scan size is $10 \mu\text{m} \times 10 \mu\text{m}$. The black colored areas in the maps for peak 4 and 5 indicate the absence of the particular Raman band in the collected spectrum.

FIGURES

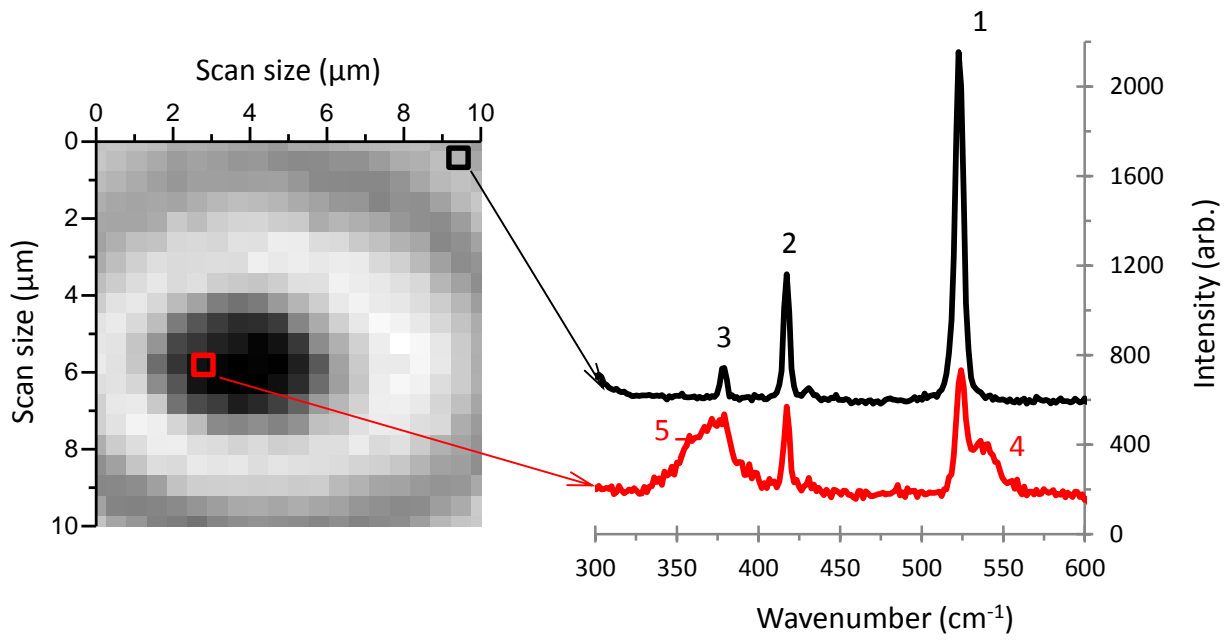


FIGURE 1

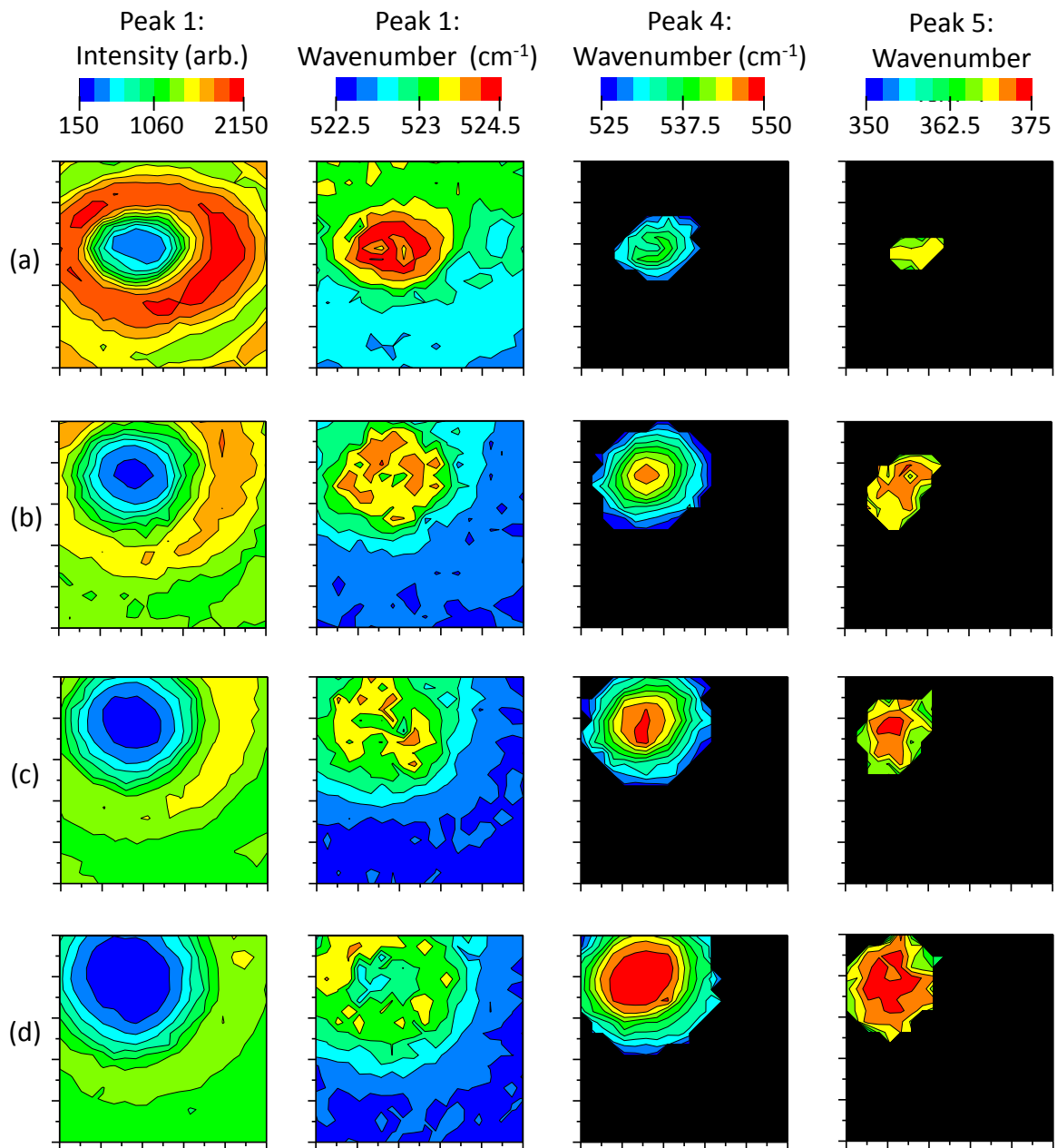


FIGURE 2